Comparison of Error Mitigation Strategies in a Hydrogen Molecule Quantum Simulation

THESIS

submitted in partial fulfillment of the
requirements for the degree of

MASTER OF SCIENCE
in
PHYSICS

Author :	BSc. X. Bonet-Monroig
Student ID :	1862081
Supervisor :	Prof.dr. C.W.J. Beenakker
	MSc. T.E. O'Brien
2^{nd} corrector :	Dr. V. Cheianov

Leiden, The Netherlands, May 28, 2018

Comparison of Error Mitigation Strategies in a Hydrogen Molecule Quantum Simulation

BSc. X. Bonet-Monroig

Instituut-Lorentz for Theoretical Physics
P.O. Box 9506, 2300 RA Leiden, The Netherlands

May 28, 2018

Abstract

Quantum simulations of molecules and exotic materials are pointed as the killer application for the next generation of quantum computers. State-of-the-art technology already allows to perform such simulations for small systems with inaccurate results. Reducing the errors of these results with error mitigation techniques is an active area of research. In this thesis, we model a quantum simulation experiment of the hydrogen molecule with a hybrid quantum-classical algorithm. The goal is to compare the performance of a combination of three error mitigation strategies, including a newly developed strategy, parity verification. We show that it is possible to obtain estimates for the dissociation curve of the hydrogen molecule below a threshold value named chemical accuracy. The conclusions presented in this thesis lay the groundwork for future experiments with larger systems in which error mitigation will be crucial to obtain meaningful results.

Contents

Chapter 1

Introduction

1.1 Quantum computing and quantum chemistry

The theory of quantum mechanics describes Nature at its smallest scale. Its predictions, which have been extensively proved experimentally, are fundamentally different with respect to classical mechanics. Such a fundamental difference led Richard Feynman to postulate that if information could be processed using quantum mechanics, it would lead to an absolutely different theory of information processing [1]. This conjecture opened to door to a new research area, namely quantum computation and information. A quantum computer is the device that carries and manipulates quantum information.

Improved fabrication and experimental control of quantum processors have permitted to move from theoretical proposals to practical applications. In this context, quantum chemistry has emerged as one of the most promising fields for which near- and mid-term quantum computers can make an impact. It is expected that these devices will solve the molecular electronic structure problem more accurately than classical computers.

In this chapter, we introduce the basic concepts of quantum computation and how they can be used to solve complex quantum mechanical problems. In particular, we describe how to express a molecular electronic structure Hamiltonian in the quantum computer language.

1.1.1 Fundamentals of quantum computing

In a quantum computer the information is stored and processed in a fundamentally different way than its classical counter-part. The basic unit of a quantum computer is a quantum bit, or qubit, as opposed to a classical bit. The key difference between the bit and the qubit is that the former can only store either a 0 or a 1, whereas the latter can be both 0 and 1 simultaneously. Therefore, the state of a qubit is described as a linear combination of 0 and 1 as:

$$|\psi\rangle = \alpha\,|0\rangle + \beta\,|1\rangle\,, \tag{1.1}$$

where α, β are complex numbers which give the probability of measuring (0,1). As the total probability of the state can not be larger than 1, it follows that $|\alpha|^2 + |\beta|^2 = 1$. The information is hence stored in a two-dimensional complex vector space. The states $|0\rangle$ and $|1\rangle$ form an orthonormal basis such a vector space, commonly referred as the computational basis. This description extends naturally to a representation of N qubits on a $\mathbb{C}^2$ via the tensor product.

In order to manipulate the state of a qubit, we need to apply quantum operations. A quantum operation $\hat{U}$ transforms the state of a qubit from $|\psi\rangle$ to $|\tilde{\psi}\rangle$ such that:

$$|\tilde{\psi}\rangle = \tilde{\alpha}\,|0\rangle + \tilde{\beta}\,|1\rangle\,. \tag{1.2}$$

A transformation of this form requires the operation to be a 2×2 matrix acting on the qubit vector space. Moreover, the fact that $|\tilde{\alpha}|^2 + |\tilde{\beta}|^2 = 1$ implies that the operation must be a unitary, $UU^\dagger = I$. A unitary matrix is therefore the quantum counter-part to a "gate" on a classical computer.

Finally, the information stored in a quantum computer must be extracted by measuring the state of the qubit. In quantum mechanics, such a process is describe by Born's rule: the output of an observable $\hat{O}$ on the state $|\psi\rangle$ is equal to one of the eigenvalues λ_i of $\hat{O}$

$$\hat{O}\,|\lambda_i\rangle = \lambda_i\,|\lambda_i\rangle\,, \tag{1.3}$$

with probability

$$P(\lambda_i) = |\langle \lambda_i | \psi \rangle|^2. \tag{1.4}$$

When a qubit is measured in a quantum computer, there are only two possible outputs, namely 0 or 1. Based on Born's rule, the observable of a qubit must necessarily be a matrix with two different eigenvalues. In a quantum computer such observables are the so-called Pauli matrices. In the computational basis, the Pauli matrices $\{X,\ Y,\ Z\}$ take the following form:

$$X = \begin{bmatrix} 0 & 1 \\ 1 & 0 \end{bmatrix}; \quad Y = \begin{bmatrix} 0 & -i \\ i & 0 \end{bmatrix}; \quad Z = \begin{bmatrix} 1 & 0 \\ 0 & -1 \end{bmatrix}$$

The fact that all these three matrices have the same eigenvalues allows us to use any of them as a basis to readout a qubit. Because the Z Pauli matrix is diagonal in the computational basis, it is generally used to measure the qubits. Measurement in the X or Y basis is performed by pre-rotations. On individual qubits, the Pauli operators anti-commute,

$$\{X, Y\} = \{X, Z\} = \{Y, Z\} = 0, \tag{1.5}$$

but acting on separate tensor factors commute:

$$[A \otimes \mathcal{I}, \mathcal{I} \otimes B] = 0, \tag{1.6}$$

for any $A, B = X, Y, Z$.

So far, we have ignored the fact that when a qubit in a superposition is measured, only partial information of its state is recovered. If we want to reliably know the values α and β, we must repeatedly prepare and measure individual experiments to accumulate statistics [2], this is known as single-shot measurements.

1.1.2 Molecular electronic structure Hamiltonian

The molecular electronic structure Hamiltonian describes the interaction between electrons and nuclei in a Coulomb potential [3]. The dynamics of a system are represented by the position of the electrons r_i and the position, mass and charge of the nuclei R_i, M_i, Z_i. The molecular structure Hamiltonian in the first-quantization formalism is given by:

$$\begin{aligned}\mathcal{H} = &- \sum_i \frac{\nabla^2_{R_i}}{2M_i} - \sum_i \frac{\nabla^2_{r_i}}{2} - \sum_{i,j} \frac{Z_i}{\left|R_i - r_j\right|} \\ &+ \sum_{i,j>i} \frac{Z_i Z_j}{\left|R_i - R_j\right|} + \sum_{i,j>i} \frac{1}{\left|r_i - r_j\right|}.\end{aligned} \tag{1.7}$$

Within the realm of quantum chemistry, this Hamiltonian is of central interest because almost all properties of the dynamics of a molecule are determined by its eigenstates.

For example, a chemical reaction occurs when the system evolves from one to another stable chemical structure. The energy difference between two stable configurations determine the kinetics of the reaction [4]. Mathematically, this is expressed in equation 1.7 by the evolution of the electrons with respect to each other and the nuclei. Those configurations that minimize the energy are the most likely to be part of the reaction mechanism. For this reason, accurate calculations of the ground and some excited state energies of this Hamiltonian are important to understand complex chemical reaction processes.

Classical computational methods have been extensively used to solve a wide range of electronic structures problems, from molecules to materials. However, for a system with hundred correlated electrons, the accuracy of these techniques no longer allows one to make reliable predictions. The reason is that the number of bits required to store all the information is $\sim 2^{100}$, exceeding the capabilities of the best supercomputers. In contrast, a quantum computer will be able to store the information in a superposition state which will drastically reduce the resources to simulate such problems.

In the last decade, there has been an effort to estimate the number of

qubits required to simulate quantum systems which exceed the capabilities of the best classical computers. Large molecules or strongly correlated materials are amongst the most studied problems in the field [4–8]. For instance, Reiher et al. [4] studied the open problem of biological nitrogen fixation. They predicted that a qualitatively valid result would require $\sim 10^4 - 10^6$ physical qubits and a computational time of the order of days including quantum error correction. A recent work by Babbush et al. [8] used a clever choice of the molecular basis to express the molecular structure Hamiltonian, which reduced the required quantum resources. They proposed jellium as a model to study in near-term quantum device including error mitigation methods instead of costly quantum error correction codes.

1.1.3 From quantum chemistry to qubits

In order to solve the molecular electronic structure Hamiltonian (eq. 1.7) on a quantum computer, we must express it in terms of qubits. Previous works have directly mapped eq. 1.7 onto a quantum computer [6]. However, in this work we use the second quantization formalism before mapping the Hamiltonian onto qubits. We follow the description given in reference [7] to express the molecular structure Hamiltonian in the second quantization formalism.

The first step to transform eq. 1.7 is to take the Born-Oppenheimer approximation, assuming that the motion of the electrons is much faster than the motion of the nuclei. The latter can, therefore, be treated as a classical point charge. Next, a basis to represent the wave-function of the electrons $\phi_i(r_i, s_i)$ is chosen with a defined position r_i and spin s_i for each electron. The position and momentum of the electrons are then expressed in terms of the annihilation and creation operators ($a_i,\ a_i^\dagger$), which obey the fermionic anti-commutation relations:

$$\begin{aligned} \{a_i, a_j^\dagger\} = a_i a_j^\dagger + a_j^\dagger a_i = \delta_{i,j}, \\ \{a_i, a_i^\dagger\} = \{a_j, a_j^\dagger\} = 0. \end{aligned} \tag{1.8}$$

The above gives the expression for the Hamiltonian:

$$\mathcal{H} = \sum_{pq} h_{pq} a_p^\dagger a_q + \frac{1}{2} \sum_{pqrs} h_{pqrs} a_p^\dagger a_q^\dagger a_r a_s, \tag{1.9}$$

where the coefficients h_{pq} and h_{pqrs} are calculated from:

$$h_{pq} = \int dr ds \, \phi_p^*(r,s) \Big[\frac{\nabla_r^2}{2} - \sum_i \frac{Z_i}{|R_i - r|} \Big] \phi_q(r,s), \tag{1.10}$$

$$h_{pqrs} = \int dr_1 ds_1 dr_2 ds_2 \, \frac{\phi_p^*(r_1,s_1)\phi_q^*(r_2,s_2)\phi_s(r_1,s_1)\phi_r(r_2,s_2)}{|r_1 - r_2|}. \tag{1.11}$$

The potential advantage of a quantum computer over its classical counterpart in simulating molecular structure problems comes from the fact that spin-orbitals can be identified with qubits. This is because a spin-orbital contributes a 2-dimensional Hilbert space tensor factor, which is precisely what a qubit does. Although some theoretical requirements exist for the realization of a qubit [9], in principle any quantum mechanical two-level system can be used as a one.

A qubit is described in terms of Pauli matrices which follow the commutation relations previously given in equation 1.6. Hence, a natural way to simulate a Hamiltonian in a quantum computer is in terms of such operators. Mapping the molecular structure Hamiltonian from its anti-commuting fermionic operators $(a, a^\dagger)$ onto a qubits is a non-trivial task.

There exist different ways in which this mapping can be done, namely the Jordan-Wigner and the Bravyi-Kitaev transformations. Both provide a recipe to write the anti-commuting fermionic operators as a linear combination of Pauli matrices such that the anti-commutation relations are preserved.

1.2 Quantum simulations

One of the applications that Feynman envisioned for quantum computers was the possibility to simulate complex quantum phenomena [1]. As

described by Seth Lloyd in [10], a quantum simulation consists of reproducing the dynamics of a quantum system by another quantum system. The requirement for such a calculation is that the interactions of the quantum system must be controllable experimentally. In other words, we must have the ability to apply quantum gates to reproduce the problem under investigation.

Recent methods that combine quantum and classical resources have emerged as an optimization of classical and quantum computation. In this hybrid quantum-classical paradigm, the computational effort is split between quantum and classical resources. A quantum computer performs those tasks that are more efficient or even impossible to do in a classical computer. In the same way, a classical computer runs those processes which a quantum computer finds difficult.

1.2.1 Variational quantum eigensolver

In the context of quantum-classical algorithms, the variational quantum eigensolver (VQE) [11, 12] has emerged as a candidate to use in the next generation of quantum hardware.

The VQE algorithm can be outlined in the following steps [12]:

1. Prepare a quantum state, $\left|\psi(\vec{\theta})\right\rangle = U(\vec{\theta})\left|\vec{0}\right\rangle$, depending on a set of parameters $\vec{\theta}$. These parameters must be experimentally adjustable in the quantum hardware.

2. Measure the energy $E(\vec{\theta}) := \left\langle\psi(\vec{\theta})\right|\mathcal{H}\left|\psi(\vec{\theta})\right\rangle$ of the state.

3. Minimize $E(\vec{\theta})$ as a function of the parameters $\vec{\theta}$ with a classical routine.

The variational principle is used to approximate the expectation value of an observable given a trial wave-function $\left|\psi(\vec{\theta})\right\rangle$, commonly named ansatzes. The variational principle states that the expectation value of a given observable with respect to a wave-function is always greater or equal to the lowest eigenvalue of an observable. If one is interested in the the ground state energy of a system, as in our case, it translates to

$$E(\vec{\theta}) \geq E_0. \tag{1.12}$$

This implies that the classical minimization routine can only push our energy closer to the ground state energy.

Some fundamental limitations of the variational methods must be taken into account while designing a VQE experiment. First, the ansatzes are problem-dependent. They are required to have sufficient overlap with the ground state eigenvector$|\psi_0\rangle$, such that the optimization of the parameters gets close to the exact solution. Unless $\left|\psi(\vec{\theta})\right\rangle = |\psi_0\rangle$ for some $\vec{\theta}$, the minimum energy $E(\vec{\theta})$ will be strictly larger than E_0. Moreover, covering the entire Hilbert space with $\left|\psi(\vec{\theta})\right\rangle$ requires an exponentially large number of parameters $\vec{\theta}$. Therefore, the computation time of the optimization routine might become extremely large [13].

Nevertheless, the fact that quantum resources are used in the VQE algorithm allows one to prepare ansatz which cannot be, in principle, computed in a classical computer. In particular, trial states which are parametrized by the action of a unitary matrix on a state, emerge naturally in a quantum computer and might not have any classical correspondence [14]. The ability to construct such states opens a window to explore problems for which classical methods ado not achieve reliable results.

The VQE algorithm has been successfully applied experimentally in the context of quantum simulations of small molecules [11, 15, 16]. These experiments use very different choices of ansatz: for instance, O'Malley et al. [15] used the unitary coupled cluster (UCC) ansatz taken from the coupled cluster method in computational chemistry. By contrast, Kandala et al. [16] designed an ansatz based on the capabilities of their quantum devices: choosing the more accurate quantum gates that could be performed experimentally.

Both, adaptability and access to new trial states make the VQE algorithm a candidate to show an advantage with respect to classical computers for quantum chemistry problems in the near- and mid-term.

1.2.2 Variational algorithms over other methods

The following quote by Frank Wilczek encompasses the long-time belief that quantum computers will help to solve problems in research areas that will directly impact society:

> "In the 21st century quantum computers will do for molecular design what classical computers did for aircraft design in the 20th century"

To fulfill these expectations, we must show that the upcoming quantum algorithms match or improve upon the best classical algorithm. Quantum chemistry and correlated electron problems have been largely studied using *ab initio* methods developed in computational chemistry. Solving those problems with quantum algorithms allows their capabilities to be benchmarked against state-of-the-art computational methods. Some of the most important computational chemistry techniques are:

- **Hartree-Fock:** This method describes the motion of single electrons in the field of the nuclei and the average field of the other electrons [17]. However it does not account for electron correlations, thus it does not provide good results for strongly correlated systems.

- **Density functional theory (DFT):** In DFT, the problem of interacting electrons in an static potential is reduced to a problem of non-interacting electrons moving in an effective potential [18]. Although DFT has been applied to study large systems of electrons with great success, the results become inaccurate when the problem involves strong correlations. Furthermore, DFT does not allow for the estimation or bounding of the errors.

- **Configuration interaction/Full configuration interaction (CI/FCI):** These are an extension of the Hartree-Fock method in which unoccupied excited orbitals are mixed with the Hartree-Fock orbitals. The CI only considers a finite number of excitations. When all the N-fold excited orbitals are taken into account (FCI) the result is the exact solution within the Born-Oppenheimer approximation [18]. The computational resources needed to solve a problem in the FCI are prohibitive, making it impossible to be used for large systems. It is expected that simulation using FCI can be efficiently performed with quantum resources.

- **Coupled Cluster (CC):** In this method the excitation operator that promotes electrons from occupied to excited orbitals is exponentiated. The CC ansatzes are prepared by the action of this exponential operator acting on the vacuum [19].

- **Other methods:** Monte-carlo and Density-matrix renormalization group are the most advanced classical methods. They show good results for strongly correlated systems but are computationally intensive if one aims to get small errors for systems with 50 electrons and beyond.

- **Quantum phase estimation algorithm (QPE):** The QPE algorithm is designed to find the phase that a unitary transformation adds to its eigenstates. It is expected that for large enough steps of the algorithm the result converges to the true eigenvalue of the unitary. However, the existing theoretical proposals require quantum error correction for large systems with the current error rates [7].

VQE has been marked as a promising algorithm to show advantage over classical methods in the near-term [12, 13]. In particular, it is hoped that simulation of ~ 50 correlated electrons might be achieved without quantum error correction [8]. Also, VQE circuits are expected to be far smaller in depth than those required for QPE .

Chapter 2

Modeling the hydrogen molecule quantum simulation

2.1 The hydrogen molecule

The hydrogen molecule (H_2) is a good first toy model for studying quantum algorithms applied to quantum chemistry. Despite its simplicity, it provides a playground to experimentally test and benchmark the capabilities of small quantum devices.

If we are to simulate the hydrogen molecule in a quantum computer, it is necessary to find the number of qubits required to experimentally do so. In quantum chemistry, qubits are identified with spin-orbitals. Hence, for H_2, where the 2 ls spin-orbitals form a minimal basis, the number of qubits is four.

From equation 1.9, one observes that the Hamiltonian can be divided into one- and two-electron parts:

$$\mathcal{H} = \sum_{p,q=1}^{4} h_{pq} a_p^\dagger a_q + \frac{1}{2} \sum_{pqrs=1}^{4} h_{pqrs} a_p^\dagger a_q^\dagger a_r a_s = \mathcal{H}^{(1)} + \mathcal{H}^{(2)}, \qquad (2.1)$$

where the integrals h_{pq} (eq. 1.10) and h_{pqrs} (eq. 1.11) depend upon the

bond length (d) between the two hydrogen atoms. The minimal basis to represent the hydrogen molecule requires to add the 4 spin-orbitals in the previous expressions.

Following the calculation by Whitfield et al. [7], the one-electron Hamiltonian is of the form:

$$\mathcal{H}^{(1)} = h_{11}a_1^\dagger a_1 + h_{22}a_2^\dagger a_2 + h_{33}a_3^\dagger a_3 + h_{44}a_4^\dagger a_4, \tag{2.2}$$

and the two-electron Hamiltonian:

$$\begin{aligned}\mathcal{H}^{(2)} = h_{1221}a_1^\dagger a_2^\dagger a_2 a_1 + h_{3443}a_3^\dagger a_4^\dagger a_4 a_3 + h_{1441}a_1^\dagger a_4^\dagger a_4 a_1 + \\ h_{2332}a_2^\dagger a_3^\dagger a_3 a_2 + (h_{1331} - h_{1313})a_1^\dagger a_3^\dagger a_3 a_1 + (h_{2442} - h_{2424})a_2^\dagger a_4^\dagger a_4 a_2 + \\ h_{1423}(a_1^\dagger a_4^\dagger a_2 a_3 + a_3^\dagger a_2^\dagger a_4 a_1) + h_{1243}(a_1^\dagger a_2^\dagger a_4 a_3 + a_3^\dagger a_2^\dagger a_4 a_1) + \\ h_{1423}(a_1^\dagger a_4^\dagger a_2 a_3 - a_3^\dagger a_2^\dagger a_4 a_1) + h_{1243}(a_1^\dagger a_2^\dagger a_4 a_3 - a_3^\dagger a_2^\dagger a_4 a_1).\end{aligned} \tag{2.3}$$

Next, one expresses the above equation in terms of operators which can be measured on a quantum computer, this is, mapping the anti-commuting fermionic operators onto Pauli operators. In this work, we use the Bravyi-Kitaev (B-K) transformation [20], which results in the following form at each bond length (d) [21]:

$$\begin{aligned}\mathcal{H} = f_0 I + f_1 Z_0 + f_2 Z_1 + f_3 Z_2 + f_1 Z_0 Z_1 \\ + f_4 Z_0 Z_2 + f_5 Z_1 Z_3 + f_6 X_0 Z_1 X_2 + f_6 Y_0 Z_1 Y_2 \\ + f_7 Z_0 Z_1 Z_2 + f_4 Z_0 Z_2 Z_3 + f_3 Z_1 Z_2 Z_3 \\ + f_6 X_0 Z_1 X_2 Z_3 + f_6 Y_0 Z_1 Y_2 Z_3 + f_7 Z_0 Z_1 Z_2 Z_3.\end{aligned} \tag{2.4}$$

Here, I_i, X_i, Y_i, Z_i are the Pauli matrices acting on the i-th qubit, and $X_i Z_j = X_i \otimes Z_j$ refers to the tensor product of the operators. The coefficients f_i are calculated from equation 1.10 and 1.11. We use the open-source package for quantum chemistry on a quantum computer OpenFermion [22] to calculate these coefficients.

A careful examination of the above Hamiltonian (eq. 2.4) leads to the observation that the operators $Z_1 Z_3$ commute with it. With this symmetry

it is possible to solve the problem in a single simultaneous eigenspace of Z_1 and Z_3. As the true ground eigenstate of H_2 is guaranteed to have non-zero overlap with the Hartree-Fock state $|0000\rangle$, it must lie in the $+1$ eigenspace of Z_1 and Z_3. By using this symmetry we can effectively reduce the full Hamiltonian from four to two qubits, leaving:

$$\mathcal{H} = g_0 I + g_1 Z_0 + g_2 Z_1 + g_3 Z_0 Z_1 + g_4 X_0 X_1 + g_5 Y_0 Y_1, \tag{2.5}$$

where the coefficients g_i are calculated from the two- and four-body integrals (1.10,1.11) and depend upon the bond length.

2.2 VQE algorithm for the hydrogen molecule

In the rest of this section, we present a VQE algorithm in a hybrid quantum-classical architecture for the hydrogen molecule, and detail the measurement protocol.

The VQE algorithm can be split into two parts, one involving quantum resources and one with a classical computer. In the quantum part, a small quantum computer is used to prepare and measure a quantum state. We differentiate between the state preparation and the measurement, although experimentally they act as one. The data processing is done in the classical section: the coefficients g_i are calculated, the expectation value is obtained as a weighted sum of individual Hamiltonian terms 2.5, and a minimization routine is launched to suggest new parameters. This is repeated until the parameters converge to a set of values which represent the approximated ground state energy, $E(\vec{\theta})$.

At the same time that we are searching for interesting problems to solve on a quantum computer, we are also interested in understanding which trial states can be efficiently prepared in small quantum devices. For instance, it is known that the Hilbert space of N-qubits can be parametrized with $p = 2^{N+1} - 2$.

However, if some physical constraints of the system are known, we can use it to reduce the number of parameters ($\vec{\theta}$) in the VQE algorithm (e.g. : conservation of particle number, conservation of parity, or real-valued

Hamiltonian). If one aims to use a VQE algorithm to simulate large systems, taken advantage of the symmetries will be important to minimize the computational resources required for it.

2.2.1 Ansatz preparation

A general 2-qubit system requires $p = 2^3 - 2 = 6$ variables to parameterize its Hilbert space. The hydrogen molecule Hamiltonian (2.5) contains only real values, hence half of the parameters are needed to reach its ground state. We can fix one more parameter by enforcing that the ground state energy of the hydrogen molecule lies in the single-excitation manifold. With all of the above, we find that only two parameters are needed in our algorithm.

The circuit that prepares the state is given in figure 2.1. In order to prepare the state in the single-excitation manifold, we apply a single-qubit rotation $R_y(\pi)$. Qubits are entangled with a parametrized two-qubit $iSwap(\theta_1)$ gate [23]. Finally, a parametrized single-qubit rotation $R_z(\theta_2)$, that accounts for any imaginary terms of the Hamiltonian, is applied. Although this circuit prepares a trial state that can be used for any Hamiltonian with real and imaginary values, for the hydrogen molecule problem, which has only real entries, the parametrized Z-rotation is unnecessary to obtain its ground state. Nonetheless, we leave it as a free parameter to observe its experimental behaviour.

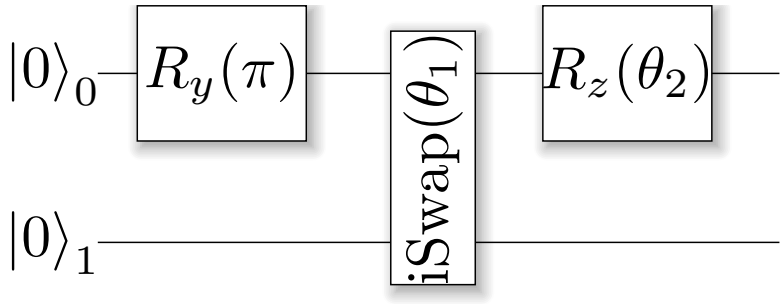

Figure 2.1: *State preparation circuit parametrized by angles θ_1 & θ_2. Qubits are initialized in the $|00\rangle$ state because its experimental preparation is simple.*

Each term of the two-qubit Hamiltonian is measured by preparing the state with the same parameters θ_1, θ_2. When the energy expectation value is calculated, an optimization process suggests a new value for the angles.

This optimization is repeated until the energy converges to a minimum at $\vec{\theta}_{\min}$ At this point, $\left|\psi(\vec{\theta}_{\min})\right\rangle$ represents the best estimate of the ground state wave-function. This is repeated for different bond lengths until the dissociation curve is clearly defined. We make use of the Nelder-Mead optimization method through the open source python software SciPy [24, 25].

2.2.2 Measurement

Previously in the text, we have described how to extract the information in a quantum computer. We have mentioned that the state of a qubit is obtained by measuring the Z observable, and also that only partial information of it can be recovered. Therefore, multiple repetitions of the measurement are needed to statistically recover the qubit state.

Measuring I, Z_0, Z_1, Z_0Z_1 is trivial because they are diagonal in the Z-basis. Furthermore, the fact that all of them commute with each other allow us to use the same single-shot measurements for obtaining their expectation values. By contrast, measuring X_0X_1 and Y_0Y_1 requires pre-rotating the qubit. This allows us to put the qubit in the X or Y basis before reading it out. The extended measurement circuit for these observables is shown in figure 2.2.

From the repeated single-shots, the density matrix of the state is reconstructed and the operators measured as:

$$\left\langle \hat{O} \right\rangle = tr[\hat{O}\rho]. \tag{2.6}$$

The expectation value of the Hamiltonian is then obtained from the individual expectation values as:

$$\langle H \rangle = g_0 \langle I \rangle + g_1 \langle Z_0 \rangle + g_2 \langle Z_1 \rangle + g_3 \langle Z_0Z_1 \rangle + g_4 \langle X_0X_1 \rangle + g_5 \langle Y_0Y_1 \rangle . \tag{2.7}$$

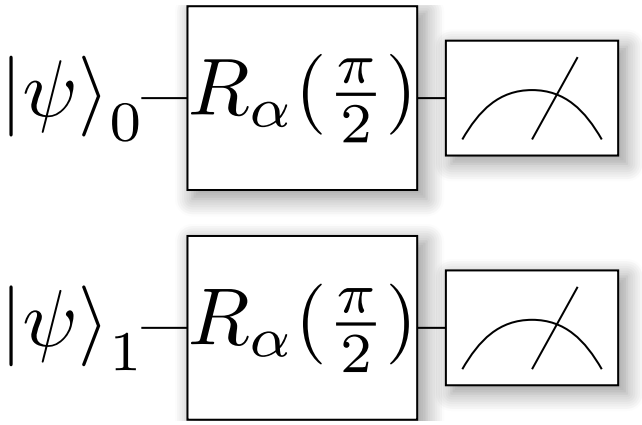

Figure 2.2: *Measurement circuit for X_0X_1 & Y_0Y_1. Here, $\alpha = Y, X$ labels the rotation to be applied.*

2.3 Simulating experimental noise

In this section, we outline the underlying error model of our numerical calculations. They have been performed using the quantumsim density matrix simulator package [26]. This software allows us to introduce a noise model to describe the qubit architecture imperfections. We use the noise model described by O'Brien et al. [27] for the superconducting transmon qubit architecture [28, 29].

One of the goals of this project is to predict the performance of an existing superconducting qubit device. We have chosen parameters to best model this device within the capabilities of quantumsim (see table 2.1).

Superconducting qubits are prone to errors due to qubit relaxation and dephasing (T_1, T_2), as well as imprecisions of control hardware (e.g. angle dephasing) and readout infidelity. The values of T_1 and T_2 have been experimentally obtained, whilst the rest of the parameters are taken from the literature and internal experimental results.

2.3.1 Idling qubits

When a qubit in the state $|1\rangle$ is idling for a time t it has a probability p_1 to decay to $|0\rangle$. If the qubit is in a superposition, it can acquire a random quantum phase with probability p_ϕ due to 1/f or broadband noise. These

probabilities depend on the qubit relaxation and dephasing time T_1, T_ϕ as:

$$\begin{aligned} p_1 &= \exp\left(-\frac{t}{T_1}\right), \\ p_\phi &= \exp\left(-\frac{t}{T_\phi}\right), \end{aligned} \tag{2.8}$$

where T_ϕ is related to the experimental values T_1, T_2 as:

$$\frac{1}{T_2} = \frac{1}{T_\phi} + \frac{1}{2T_1}. \tag{2.9}$$

2.3.2 Single-qubit gates

Single-qubit gates are modeled as an instantaneous gate sandwiched by idling gates of time $t = \frac{\tau_{1Q}}{2}$. In this way, it is possible to separate errors due to qubit decoherence from those related to hardware control imperfections.

The instantaneous R_y rotation gate is modeled with an additional depolarizing noise which corresponds to a shrink towards the origin of the Bloch sphere. The size of this errors is p_{axis} along the y-axis and p_{plane} in the x,z-plane. On the other hand, the instantaneous R_z rotation will only suffer from an over-rotation of the axis $(1 - p_{axis})$.

2.3.3 Two-qubit gates

The model for two-qubit gates is the same as the single-qubit model; two-qubit gates are applied instantaneously, and sandwiched between two idling gates of time $t = \frac{\tau_{2Q}}{2}$. In general, quantumsim allows one to independently set the one- and two-qubit gate times. In our simulations we have set the time to $\tau_{2Q} = 2\sqrt{2}\tau_{1Q}$, provided by experimental collaborators.

Unlike the single-qubit case, which is modeled from experimental tomography, the instantaneous noisy two-qubit gate has a model based on

the understanding of underlying physical error mechanisms. In our algorithm, we use two of these gates with different noise models [23].

1. **iSwap**: The gate is used to prepare the trial state in its parametrized version. Experimentally this is performed by holding the system for a time $\tau(\theta)$ in the $|01\rangle \leftrightarrow |10\rangle$ avoided crossing such that the excitations are exchanged between the qubits (process matrix given in app. A.). The imperfection on the application of the angle is accounted for by including a small incoherent error in the angle value.

2. **CNOT**: Experimentally this gate is decomposed in two single-qubit gates and two-qubit C-Z gate (detailed in app. A). The C-Z gate is performed by holding the system for a time τ_{2Q} at the avoided crossing $|11\rangle \leftrightarrow |02\rangle$. The state $|01\rangle$ acquires a phase which is multiple of 2π , whilst the state$|11\rangle$ picks up a phase which is an odd multiple of π , as required. Inaccuracies on the phase acquisition are modeled with a small incoherent deviation from the expected phase value. The dephasing parameter is taken from the supplementary material of reference [27].

2.3.4 Measurement

The implementation of the measurement process in our simulations largely differs from the physical realization. Instead of reconstructing the density matrix of the system from single measurements, we extract it from quantumsim without collapsing the state. The expectation values are calculated as in equation 2.6. This is justified because the error in measurement can be canceled by careful tomography using linear inversion or maximum likelihood estimation techniques, with one exception: sampling noise.

Through the text, we have emphasized that to accurately describe the qubit state, it is necessary to measure it multiple times. However, for the sake of simplicity, in our numerical simulation we have completely omitted this the error introduced by the finite number of measurements performed in a real experiment.

Table 2.1: *Values used in the simulations.*

Parameter	QL	QR
T_1	9.8 μs	10.8 μs
T_2 echo	9.4 μs	10.4 μs
τ_{1Q}	20 ns	20 ns
τ_{2Q}	$\sqrt{2}\cdot$ 40 ns	$\sqrt{2}\cdot$ 40 ns
In-axis dephasing	10^{-4}	10^{-4}
In-plane dephasing	$5 \cdot 10^{-4}$	$5 \cdot 10^{-4}$
iSwap dephasing	$10^{-2}/2\pi$	$10^{-2}/2\pi$
C-Z dephasing	$10^{-2}/2\pi$	$10^{-2}/2\pi$

2.3.5 Other noise channels

Even though the quantumsim package has a very accurate error model, there are noise sources that are not yet incorporated which could have significant effects on the experiment.

First of all, a more thorough noise model is needed for the two-qubit gates, including leakage effects. Leakage occurs when the qubit gets excited out of the two lowest energy levels. The C-Z gate is very sensitive to this effect since the qubit is moved close to the $|02\rangle$ state and there is a non-zero probability to tunnel to it.

Another unmodeled source of noise is qubit-qubit flux cross-talk, and microwave cross-talk. When a qubit is manipulated, neighboring qubits might interfere with it, reducing the fidelity of the process.

2.4 Results

In figure 2.3 we present the result of the simulation in the absence of error mitigation strategies. The ground energy curves are compared to the exact solution calculated from equation 2.5. In computational chemistry, the result of a simulation is often validated with respect to the chemical accuracy (CA) threshold [3], equivalent to 1.6 *mHartree*. The reason is that an error in the dissociation curve of this value translates into an error in reaction rates of one order of magnitude [3].

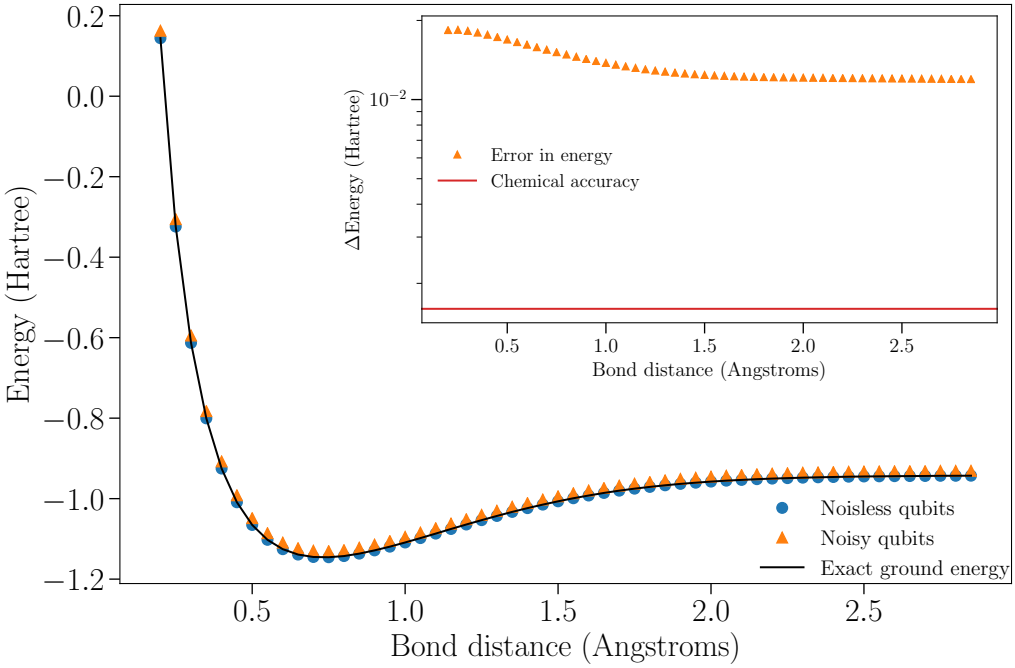

Figure 2.3: *Exact dissociation curve (solid black), solution of the VQE algorithm for noiseless (blue dots) and noisy (orange triangles) qubits. Inset: Deviation from the exact solution under noise effects and chemical accuracy line (solid red).*

We first compute the numerical calculation under the ideal scenario of a noiseless device. As expected, the exact solution fully overlaps with the simulation of the experiment (blue dots in figure 2.3). The result is a confirmation that, under ideal conditions, it is possible to calculate the ground state energy of the hydrogen molecule via quantum simulations with 2 qubits. Moreover, it confirms that the code works correctly.

Figure 2.3 additionally shows the simulation result in the presence of experimental noise (orange triangles). The inset of the figure shows the error in energy of the noisy curve with respect to the exact solution (black solid line). As a visual reference, we also include the chemical accuracy threshold (red line).

We conclude that with the available device a quantum simulation of H_2 with errors below the CA line can not be done without the assistance of error mitigation strategies.

Chapter 3

Error mitigation techniques

3.1 Introduction

In the previous chapter, we have shown that small calculations on current quantum hardware are insufficient to make predictions. For instance, a VQE quantum simulation of a molecule with 50 orbitals will require a circuit of length $\sim 10\ \mu s$, reaching the limits of our experimental device. Assuming an error probability of $p = 5 \cdot 10^{-2}$ every $1\ \mu s$, the estimate error of such a simulation is:

$$p' = 1 - (1 - p)^{t'} = 1 - (1 - 0.05)^{10} \sim 5 \cdot 10^{-1}. \tag{3.1}$$

This result shows that the current technology will not be sufficient to run large calculations. While it is expected that error rates will be reduced in upcoming generations of quantum technology, we do not expect these to be sufficiently reduced for accurate quantum simulations without additional strategies to correct or mitigate remaining errors.

Quantum error correction (QEC) is a scalable, long-term strategy to build a quantum computer that can perform fault-tolerant calculation with noisy qubits [30]. However, the requirements to apply QEC techniques with existing hardware are prohibitive. For instance, Reiher et al. [4] estimated that simulating a large molecule within chemical accuracy on a fault-tolerant quantum computer will require of the order of million physical qubits

with error rates of 0.1%.

An alternative solution for near-term quantum computers are the so-called error mitigation techniques. They use extra information accessible about the system to reach more accurate results. Error reduction methods represent an intermediate method towards accurate solutions without, or with minimal, QEC .

In this chapter, we apply three error mitigation strategies to a hydrogen molecule quantum simulation to study their performance. We introduce a new technique that we call 'parity verification', and apply to other previous developed technique: quantum subspace expansion [31] and active error minimization [32, 33]. The goal is to estimate the error reduction of these strategies for our device. Moreover, we aim to investigate their combination with the idea of reaching chemical accuracy for the H_2 dissociation curve.

3.2 Parity verification measurement

Given a physical system described by a Hamiltonian H and a conserved quantity C, if

$$[H, C] = 0, \tag{3.2}$$

we may simultaneously measure H and C. This can be used to verify that the prepared state lies in the subspace in which the desired solution is contained. Experimentally, one will disregard the outputs in which C signals an error.

By enforcing physical symmetries, it is possible to reduce noise due to the interaction between the environment and the quantum computer, also known as incoherent noise. The reason is that the effect of the noise on the state often puts it out of the correct eigenspace of C. By disregarding the measurement, we prevent the error to enter into the final result. We expect this technique to be especially effective because incoherent noise represents the main source of errors on superconducting qubits.

In the hydrogen molecule problem, there exists a conserved quantity that can be used to signal errors. The operator Z_0Z_1, which contains information about the parity, commutes with the Hamiltonian 2.5. From quantum chemistry, it is known that the ground state energy lies in the

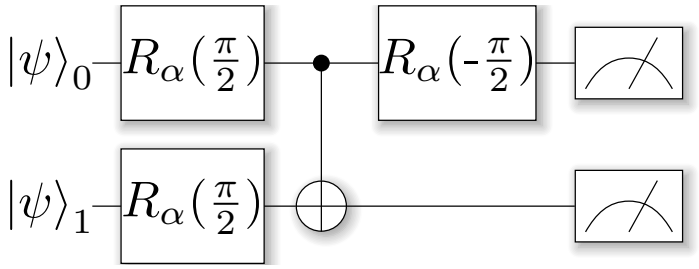

Figure 3.1: *Parity verification measurement circuit for X_0X_1 & Y_0Y_1. Here, $\alpha = Y, X$ labels the rotation to be applied.*

single-excitation manifold and, thus has odd parity. Therefore, it is possible to measure the energy and the parity and disregard those measurements that do not satisfy the correct parity. Note that a change in the parity of a state comes from a qubit flipping from the excited to the ground state. A bit-flip error like this occurs when a qubit relaxes, hence we expect to fully mitigate the T_1 noise channel.

In chapter two, we have described how the individual expectation values are calculated from single-shot measurements, as well as the expectation value of the Hamiltonian. Again, I, Z_0, Z_1 & Z_0Z_1 can be obtained from the same set of measurements. The parity is calculated from the single-shot values $a = 0, 1$ or $b = 0, 1$ of each qubit as:

$$\mathcal{P} = (-1)^{a+b}, \tag{3.3}$$

if $\mathcal{P} \neq -1$, the measurement is disregarded.

By contrast, measuring ZZ along with XX or YY requires an extension of the circuit. It is sufficient to use a single circuit because $ZZ \cdot XX = YY$. The extended measurement circuit is shown in figure 3.1. In this circuit, the parity is encoded in the top qubit, whereas the bottom one gets the information of the state. When the top qubit returns a 0, the measurement is disregarded because $\mathcal{P} = 1$.

With the parity verification (PV) technique, we would expect to cancel all the errors due to qubit relaxation. However, the need of a circuit extension incorporates noise which can not be eliminated at the end of it. Additionally, the fact that measured data needs to be thrown away might become a problem when the error probability is large, implying that this technique does not scale in the same manner as QEC .

3.3 Quantum subspace expansion

McClean et al. [31] developed the quantum subspace expansion (QSE) method to approximate excited states of a Hamiltonian from a ground state wave-function obtained with a quantum computer. The wave-function $|\psi_0\rangle$ becomes the reference state to explore the spectrum of the system by extending the Hilbert space with excitations from it. Therefore, the first excited manifold will be found by acting with a single operator on each qubit. The second will be reached by applying excitation to two qubits, and similarly for larger systems.

Mathematically, this will translate into a construction of a new set of vectors $|\phi_i\rangle$, such that:

$$|\phi_i\rangle = A_i |\psi_0\rangle , \tag{3.4}$$

where A_i are the excitations from the reference state. These vectors are then used as a basis to extend the problem Hamiltonian $\mathcal{H}$ as:

$$\tilde{\mathcal{H}}_{i,j} = \langle\phi_j| \mathcal{H} |\phi_i\rangle = \langle\psi_0| A_j^\dagger \mathcal{H} A_i |\psi_0\rangle . \tag{3.5}$$

Finally, the excited states are calculated by solving the generalized eigenvalue problem of the new Hamiltonian $\tilde{\mathcal{H}}$:

$$\tilde{\mathcal{H}} |\lambda\rangle = \lambda C |\lambda\rangle , \tag{3.6}$$

where C is the overlap matrix, given by:

$$C_{i,j} = \langle\phi_j|\phi_i\rangle = \langle\psi_0| A_j^\dagger A_i |\psi_0\rangle \tag{3.7}$$

In the same paper [31], it is shown that the ground state energy given by the $\tilde{\mathcal{H}}$ is a more accurate solution than that resulting from $|\psi_0\rangle$ alone. The argument is that the ground state energy given by a quantum computer does not belong to the problem Hamiltonian, but a different one that has been modified by errors that can be described in terms of Pauli operators. By extending the Hamiltonian with those operators, a better approximation of the ground state can be reached.

The application of QSE as a mitigation strategy requires a careful selection of the set of operators A_i to extend the problem because the number of measurements required grows polynomially with the number of operators. Moreover, prior to the start of the experimental run, one must know which extra measurements are required in the expansion.

In this work, we apply the linear response (LR) expansion, also described in reference [31], on the two-qubit H_2 Hamiltonian (eq. 2.5). The set of operators in this expansion is given by:

$$A_i = \{II, ZI, IZ, XI, IX, YI, IY\}. \tag{3.8}$$

The application of these operators on equation 2.5 leads to a 7-dimensional effective Hamiltonian $\tilde{\mathcal{H}}$. In addition to the previous expectation values, $\tilde{\mathcal{H}}$ also depends on $\langle XY \rangle$ and $\langle YX \rangle$. If we are to combine QSE with the parity verification method another measurement circuit is needed. It takes the same form of figure 3.1, with different rotation in each qubit.

In our simulations, QSE is computed as a post-processing step after the optimal set of angles have been obtained from a numerical minimization of the initial circuit. These angles define approximate the lowest eigenstate of the Hamiltonian $|\psi_0\rangle$ which is necessary to calculate the additional expectation values. Once all the terms have been measured, the effective Hamiltonian and overlap matrices are computed. Finally, the eigenvalues of these matrices are calculated and its lowest eigenvalue becomes the new energy expectation value.

It is important to mention that a first demonstration of this method to H_2 has recently been performed [34]. However, QSE has not been tested together with other mitigation techniques. We aim to show that it is possible to combine QSE with other methods to reduce the final error in the energy estimate.

3.4 Active error minimization

The last error mitigation method under study is active error minimization (AEM). It was originally introduced by Benjamin et al. [32, 35] and almost simultaneously by Temme et al [33]. They describe an algorithm to reach a

more accurate solution of the expectation value of a problem Hamiltonian $\mathcal{H}$ by running experiments with higher error rates.

At the heart of AEM lies the idea that the energy calculated from a noisy quantum computer differs from the true value as:

$$\left\langle \tilde{\mathcal{H}} \right\rangle (\epsilon) = \langle \mathcal{H} \rangle + \epsilon a_1 + \epsilon^2 a_2 + \epsilon^3 a_3 + \mathcal{O}(\epsilon^4), \tag{3.9}$$

where $\left\langle \tilde{\mathcal{H}} \right\rangle$ represents the expectation value of $\langle \mathcal{H} \rangle$ at a noise level ϵ and a_k are constants of the noise model. Therefore, ϵ can be accurately calculated as one makes the experiment progressively worse. The error-free expectation value can be obtained from a polynomial extrapolation at $\epsilon \to 0$.

Although AEM is an interesting idea to reduce the errors in a computation, its experimental implementation remains unclear. For instance, finding an experimental knob that can be controlled to increase the errors seems a challenging task. Moreover, in the case that one or more of those knobs can be found, they need to be linked to a noise source. Finally, we will not expect that detuning a single parameter will leave the other noise channels static, hence not affecting the final expectation value.

Nonetheless, we simulate the performance of AEM in our existing device. As discussed in section 2.3, this work focuses on cQED transmon qubits which are known to be coherence-limited. The largest sources of error are due to T_1 and T_2 decay during the experiment. One would expect that as the circuit time increases, so does the error in the energy because the qubits are longer exposed to decoherence. For this reason, circuit length (τ) can be used as an error parameter in equation 3.9.

In our simulations, τ is tuned by increasing the time of all single- and two-qubit gates. Based on the error model described in section 2.3, this translates into longer idling gates that expose the qubits to more errors due to decoherence. It turns out that this can be realized in our experimental set-up by adding waiting times between the gates.

We must not ignore however, that every point of the hydrogen molecule dissociation curve needs to be measured and optimized to find its lowest value. In a real experiment, such optimization currently requires ~ 4 hours for each point. A quantum simulation of 54 points will run for approximately 9 days.

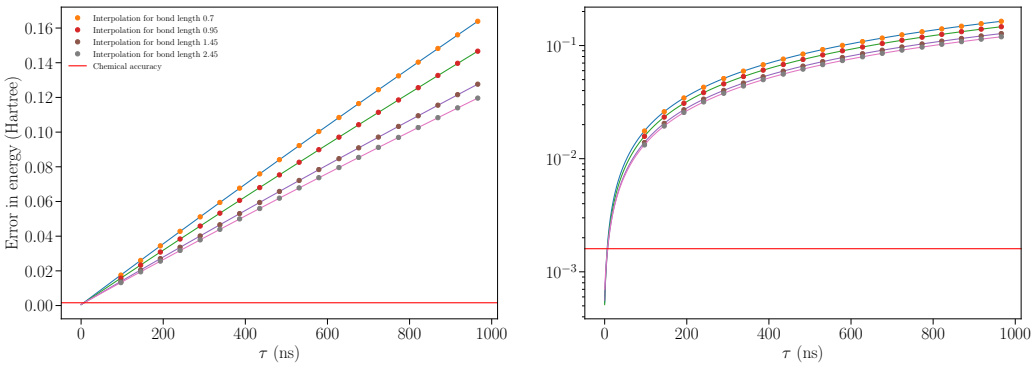

Figure 3.2: *Example of active error minimization for different bond lengths. The dots are the energy calculated from the VQE experiment at different τ, the solid line is the least-square fitting of the energies. Both left and right panels show the same data.*

The optimal angles at each point are used to compute the energy of a longer circuits. Experimentally, the computational time needed to do so is approximately one day. Each dissociation curve currently requires 1.5 hours repeated for 19 circuit lengths. In total, we estimate an experimental time of 10 days to implement AEM . Optimizing this is a key target for future research.

Nonetheless, we aim to predict the performance in our existing device, for a simulation of 54 bond distances and 19 circuit lengths. Extrapolation curves for different distances are shown in figure 3.2, in linear (left) and logarithmic (right) scales. The error-free ground state energy is computed from a third order polynomial fit of the minimum energy calculated at different τ.

3.5 Combining error mitigation techniques

The goal of this project is to benchmark the error reduction provided by the previous noise mitigation methods under current experimental parameters. Additionally, we are interested in the performance of all possible combinations of these strategies in order to reach a more accurate solution in future simulations, as well as in H_2.

3.5.1 Parity verification and QSE/AEM

The parity verification circuit together with either QSE or AEM is obtained in the same way as for the initial circuit. The ground state energy is computed from a numerical optimization of $\vec{\theta}$ with the parity verification strategy.

Next, if we want to overlay this solution with QSE, the optimal angles $\vec{\theta}_{\text{min}}$ must be fed into the post-processing stage to calculate the additional terms, compute the matrices and get the lowest eigenvalue of the extended Hamiltonian as the new energy estimate.

In a similar way as before, AEM uses $\vec{\theta}_{\text{min}}$ computed from the parity verification measurement as previously described.

3.5.2 QSE and AEM

The application of QSE and AEM is done by feeding $\vec{\theta}_{\text{min}}$ of the initial circuit into the QSE data processing. The energy at a given circuit length is obtained from the QSE lowest eigenvalue. By extracting the energy estimate from QSE at different circuit lengths, we are able to apply the AEM extrapolation.

While simulating the output of these combinations, we encountered that the lowest eigenvalue goes below the exact solution of the hydrogen molecule. As discussed in the first chapter, the variational principle ensures $E(\vec{\theta}_{\text{min}}) \leq E_0$. Hence, the result obtained does not have any physical value as it no longer corresponds to our problem Hamiltonian. Furthermore, at some bond distances the generalized eigenvalue problem can not be solved because the overlap matrix C can be made non-positive by numerical error.

In order to overtake these issues, we tried to eliminate the columns that broke the non-positivity of C. This translated into a reduction of the Hilbert space that no longer contained the ground state energies, but only excited states. As a future work, we want to solve this problem by projecting onto the positive sector of the overlap matrix.

3.5.3 Parity verification, QSE and AEM

As a final goal of this work, we simulate the combination of the three methods, aiming to push the error of the dissociation curve significantly below the chemical accuracy (CA) threshold.

The implementation requires us to obtain the optimized angles $\vec{\theta}_{\text{min}}$ from the parity verification measurement. Such angles are then used to calculate the estimate energy from the QSE protocol. This becomes the ground state energy at a given circuit length. The final energy estimate is obtained by repeating this for several circuit lengths, and getting the error-free energy from the AEM protocol.

3.6 Results

In the rest of this chapter, we show the results of the application of the error mitigation techniques to the hydrogen molecule quantum simulation.

In figure 3.3, we present the error with respect to the exact dissociation curve of a single mitigation technique. The orange dots represent the noisy experiment without error reduction.

From this plot, one already notices that QSE (purple stars) does not provide a significant improvement over the initial result. Furthermore, around $R = 0.5$Å the error shows a kink that goes above the bare VQE experiment. This is unexpected because one would assume that the lowest eigenvalue of the extended Hamiltonian will be smaller of equal to the reference ground state. A possible explanation is that the additional expectation values calculated from the optimal angles are more noisy than QSE is capable of correcting. However, a more rigorous study is required to understand the possibilities of QSE as a noise cancellation protocol.

The parity verification measurement (green stars) shows a remarkable improvement of more than an order of magnitude in the short inter-atomic distances, reaching points below the chemical accuracy (CA) (solid red line). However, for intermediate and large bond distances, the error increases by almost an order of magnitude. Such a large deviation in the curve is understood by the fact that for short distances our errors are

mainly caused by the T_1 channel, or bit-flips. By verifying the parity, we are signaling these bit-flips, and thus we are able to eliminate them.

By contrast, at large distances bit-flips are not the only errors disturbing the computation. While we can correct the remaining T_1-related errors, we are largely affected by dephasing due to T_2 decay. The reason is that larger bond lengths require more entanglement between the qubits, thus exposing the system to such noise channels. As proof, in figure 3.4 we show the expectation values of the individual terms of the two-qubit hydrogen Hamiltonian. Here, one can see that the $\langle XX \rangle = \langle YY \rangle \sim 0$ for short distances, while $\langle ZI \rangle$ and $\langle IZ \rangle$ are at their maximum value. When the distance between hydrogen atoms gets larger, $\langle ZI \rangle$, $\langle IZ \rangle$ tend to 0, but $\langle XX \rangle = \langle YY \rangle \simeq -1$. Hence, more entanglement is required to accurately measure these expectation values.

The last curve on figure 3.3 (brown stars) shows the error in the energy from the AEM protocol, as described previously. This is approximately the error in our calculation in the absence of decoherence. By only applying AEM in our experiment, we reduce the error from the initial experiment by an order of magnitude, putting the simulation below CA for the entire dissociation curve. The reason for AEM to give such an improvement is that transmon qubits are coherence-limited, thus the time to implement a circuit is the main noise channel.

We continue by presenting the combination of two techniques in figure 3.5 (purple and brown triangles). As previously discussed in this chapter, the combination of QSE and AEM have not been successful, and we do not include it in the figure.

By looking at the curve of PV and QSE (purple triangles) one notices that the correction is similar to the one given by PV alone. Again, at large bond distances dephasing is the dominant error channel and neither PV nor QSE are able to mitigate it. This simulation also suggests that PV and QSE mitigate similar noise channels.

If now we focus our attention at the PV and AEM plot (brown triangles), we observe that AEM allows us to suppress errors by almost two orders of magnitude with respect to the starting simulation. Remarkably, the three AEM curves show a similar error trend, steadily increasing with bond distance and flattening towards the end. This can be seen as AEM being the method that mitigates most of the errors.

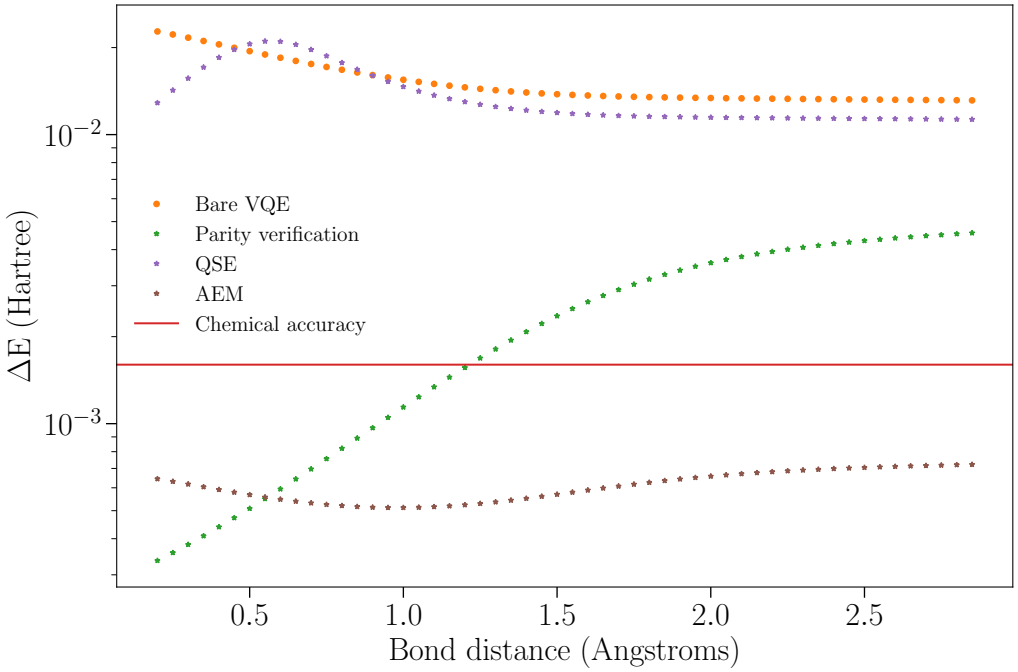

Figure 3.3: *Comparison of one mitigation technique with respect to the bare VQE experiment.*

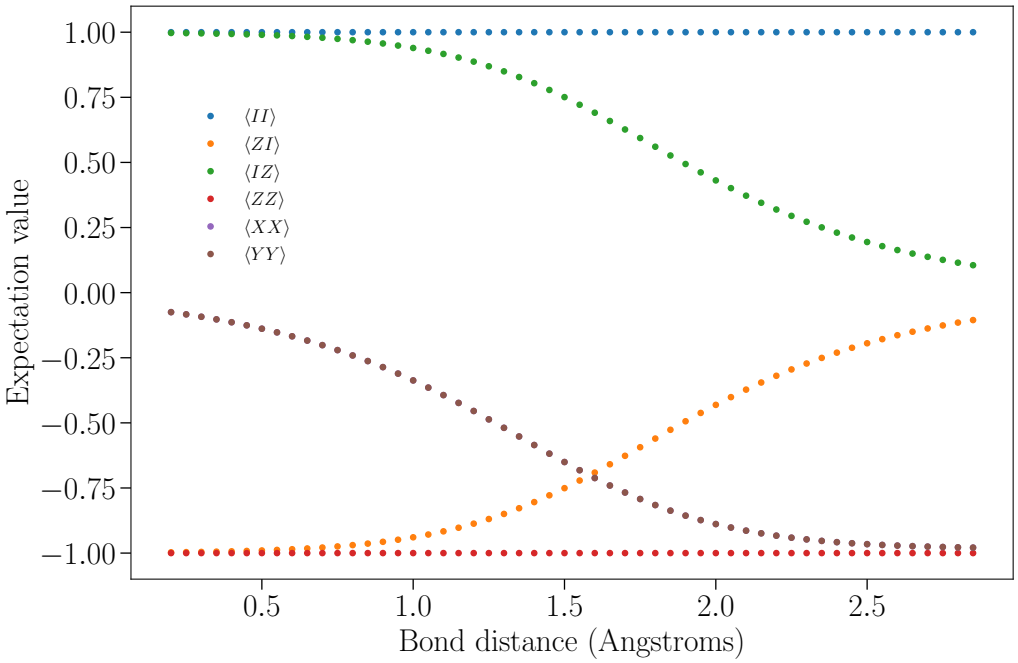

Figure 3.4: *Expectation values of H_2 Hamiltonian from the VQE experiment*

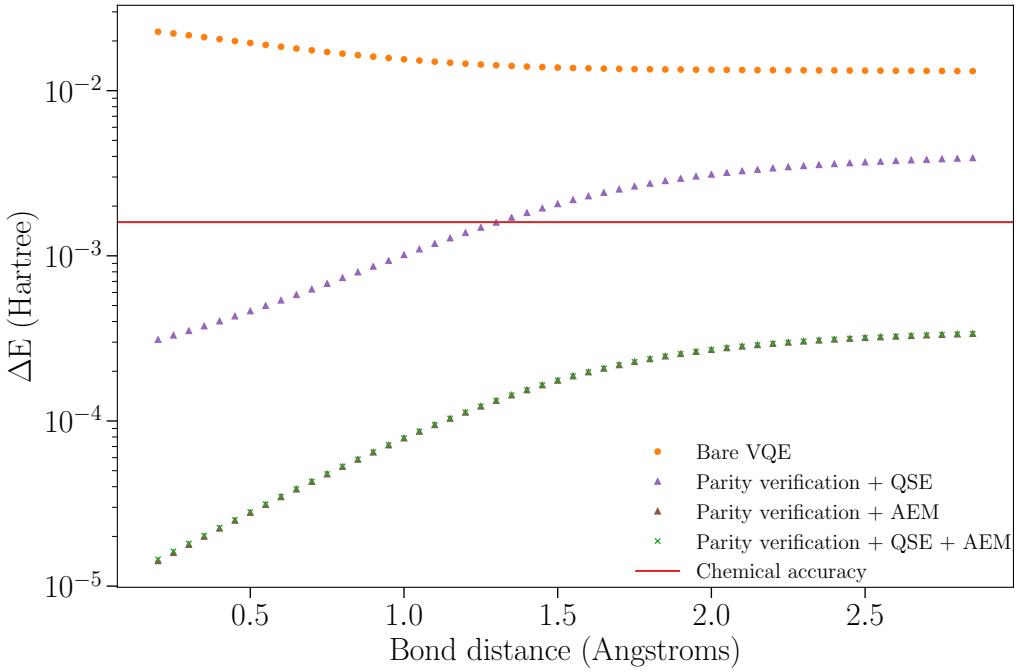

Figure 3.5: *Energy error without mitigation and with two and three mitigation methods: PV + QSE, PV + AEM, and PV + QSE + AEM*

Finally, in figure 3.5 we show the result of combining the three mitigation strategies (green crosses). We observe that the curve fully overlaps with the one of PV and AEM . This shows that QSE no longer suppresses any errors, and only parity verification and AEM are able to mitigate them.

The results seen previously suggest two relevant considerations to be made when planning VQE experiments:

1. Stacking several layers of mitigation does not guarantee a more accurate result.

2. Before running an experiment, it is important to balance between error reduction and the experimental cost of implementing these schemes.

Chapter 4

Conclusions and outlook

In this thesis we have modeled a quantum simulation experiment for the hydrogen molecule using a VQE algorithm to compare three error mitigation techniques. We have used a density-matrix quantum simulator that allows us to introduce a realistic error model based on the current state-of-the-art quantum hardware. Moreover, we have developed a new strategy to signal and eliminate errors that violate physical restrictions of the problem under study. We have further explored existing noise suppression schemes, and analyzed two of them: quantum subspace expansion and active error minimization.

Two main results have been obtained from this work. Firstly, we have estimated the performance of the VQE experiment on an existing device. We have shown that in the absence of error mitigation, it is not possible to achieve a reliable result on the dissociation curve of the hydrogen molecule. Secondly, we have explored the capabilities of the same experiment in combination with three error mitigation strategies. We have shown that near-term quantum devices can provide accurate solutions without requiring full quantum error correction.

The error mitigation strategies developed and used in this work are currently being implemented in a quantum simulation experiment in DiCarlo lab at TU Delft. As a follow up of this project, we are interested in developing tools to assist VQE algorithms, for instance a Bayesian estimator that can reduce the number of measurements needed to reach accurate results. Additionally, we aim to find new ways of reducing the error bars of VQE

and other quantum algorithms by applying existing, or newly developed error mitigation schemes.

Moreover, we would like to extend the conclusions of this thesis to study larger systems. Solving them will most likely require the assistance of classical computers in the upcoming generation of noisy devices. Hence, adapting and creating new hybrid algorithm is also very appealing for the future. Ultimately, we aim to elucidate the necessary requirements to achieve "quantum chemistry supremacy" before the quantum error correction era.

Acknowledgments

I would like to start by thanking Carlo Beenakker and Tom O'Brien for considering me as the suitable candidate for this project, although I was a constant bother at their lectures. I would like to emphasize that Tom has been an incredible supervisor from whom I learned almost everything I know about research, and also has become a very good friend.

Since my very first day at the Nanophysics group, I felt very welcomed and I rapidly became an active member of it. It is an honor, and a privilege, to work with such an extraordinary and smart group of people. I am very grateful to everyone of them: Paul, Nicandro, Maxim, Marcello, Lizzy, Yaroslav, Nikolay, Cameron, Slava, Michal, Mark, Jimmy and Marco. Thank you all for never refusing to answer my questions, and for tolerating my "peculiar" vision of life (and death).

I must not forget to include everyone at the Instituut-Lorentz that have helped me, one way or another. In particular, I am very grateful to our secretaries Fran and Manon because without them nothing would be as easy as it is.

Furthermore, I would like to express my gratitude to Leo DiCarlo and his lab for showing and teaching me the beauty of quantum mechanics in action. Brian, Niels, Adriaan, Ramiro, Malay and all the others, thank you all for making me part of what you are trying to achieve.

Last, but not least, I would like to thank my parents for constantly reminding me that hard-work is the only way to be a better person. I also like to give a special mention to my little sister, Ada, who has always been

my source of motivation to never give up such that she can see me as a role-model. Finally, the person to whom I owe the greatest gratitude is my girlfriend, Mireia. None of what I achieved in my life would have been possible without her because alone we are good, but together we are better.

Appendix A

Matrix representation of gates

Here we show the matrix representation of the gate set used throughout the text.

Pauli rotations

$$R_x(\theta) = \begin{bmatrix} \cos\left(\frac{\theta}{2}\right) & i\sin\left(\frac{\theta}{2}\right) \\ i\sin\left(\frac{\theta}{2}\right) & \cos\left(\frac{\theta}{2}\right) \end{bmatrix} \tag{A.1}$$

$$R_y(\theta) = \begin{bmatrix} \cos\left(\frac{\theta}{2}\right) & \sin\left(\frac{\theta}{2}\right) \\ -\sin\left(\frac{\theta}{2}\right) & \cos\left(\frac{\theta}{2}\right) \end{bmatrix} \tag{A.2}$$

$$R_z(\theta) = \begin{bmatrix} \cos\left(\frac{\theta}{2}\right) + i\sin\left(\frac{\theta}{2}\right) & 0 \\ 0 & \cos\left(\frac{\theta}{2}\right) + i\sin\left(\frac{\theta}{2}\right) \end{bmatrix} \tag{A.3}$$

Specific Pauli rotations

$$R_x\left(\frac{\pi}{2}\right) = \frac{1}{\sqrt{2}} \begin{bmatrix} 1 & i \\ i & 1 \end{bmatrix} \tag{A.4}$$

$$R_y\left(\frac{\pi}{2}\right) = \frac{1}{\sqrt{2}}\begin{bmatrix} 1 & 1 \\ -1 & 1 \end{bmatrix} \tag{A.5}$$

$$R_y(\pi) = \begin{bmatrix} 0 & 1 \\ -1 & 0 \end{bmatrix} \tag{A.6}$$

Two-qubit Gates

$$iSwap(\theta) = \begin{bmatrix} 1 & 0 & 0 & 0 \\ 0 & \cos\theta & i\sin\theta & 0 \\ 0 & i\sin\theta & \cos\theta & 0 \\ 0 & 0 & 0 & 1 \end{bmatrix} \tag{A.7}$$

$$CNOT = \begin{bmatrix} 1 & 0 & 0 & 0 \\ 0 & 1 & 0 & 0 \\ 0 & 0 & 0 & 1 \\ 0 & 0 & 1 & 0 \end{bmatrix} \tag{A.8}$$

In a real experiment a CNOT gate is decomposed as:

$$CNOT = [I \otimes R_y(-\frac{\pi}{2})] \cdot CZ \cdot [I \otimes R_y(\frac{\pi}{2})] \tag{A.9}$$

Where the new matrices take the following form:

$$I \otimes R_y(-\frac{\pi}{2}) = \frac{1}{\sqrt{2}}\begin{bmatrix} 1 & -1 & 0 & 0 \\ 1 & 1 & 0 & 0 \\ 0 & 0 & 1 & -1 \\ 0 & 0 & 1 & 1 \end{bmatrix} \tag{A.10}$$

$$I \otimes R_y(\frac{\pi}{2}) = \frac{1}{\sqrt{2}}\begin{bmatrix} 1 & 1 & 0 & 0 \\ -1 & 1 & 0 & 0 \\ 0 & 0 & 1 & 1 \\ 0 & 0 & -1 & 1 \end{bmatrix} \tag{A.11}$$

$$CZ = \begin{bmatrix} 1 & 0 & 0 & 0 \\ 0 & 1 & 0 & 0 \\ 0 & 0 & 1 & 0 \\ 0 & 0 & 0 & -1 \end{bmatrix} \tag{A.12}$$

Bibliography

[1] R. P. Feynman, *Simulating physics with computers*, International Journal of Theoretical Physics **21** (1982).

[2] M. Nielsen and I. Chuang, *Quantum computation and quantum information*, Cambridge University press, Cambridge, UK, 2001.

[3] T. Helgaker, P. Jorgensen, and J. Olsen, *Molecular Electronic Structure Theory*, Wiley, New York, 2002.

[4] M. Reiher et al., *Elucidating reaction mechanisms on quantum computers*, Proceedings of the National Academy of Sciences **114**, 7555 (2017).

[5] A. Aspuru-Guzik, A. Dutoi, P. Love, and M. Head-Gordon, *Simulated quantum computation of molecular energies*, Science **309** (2005).

[6] I. Kassal et al., *Polynomial-time quantum algorithms for the simulation of chemical dynanmics*, PNAS **105** (2008).

[7] J. D. Whitfield, J. Biamonte, and A. Aspuru-Guzik, *Simulation of electronic structure Hamiltonians using quantum computers*, Molecular Physics , 735 (2010).

[8] R. Babbush et al., *Low depth quantum simulation of electronic structure*, arXiv:1706.00023v3 [quant-ph] (2018).

[9] D. DiVincenzo, *The physical implementation of quantum computation*, arXiv:0002077 [quant-ph] (2000).

[10] S. Lloyd, *Universal Quantum Simulators*, Science **273**, 1073 (1996).

[11] A. Peruzzo et al., *A variational eigenvalue solver on a photonic quantum processor*, Nature Communications (2014).

[12] J. R. McClean, J. Romero, R. Babush, and A. Aspuru-Guzik, *The theory of variational hybrid quantum-classical algorithms*, New Journal of Physics (2016).

[13] N. Moll et al., *Quantum optimization using variational algorithms on near-terms quantum devices*, arXiv:1710.01022 [quant-ph] (2017).

[14] Y. Shen et al., *Quantum implementation of Unitary Couple Cluster for simulating molecular electronic structure*, Phys. Rev. A (2017).

[15] P. J. J. O'Malley et al., *Scalable Quantum Simulation of Molecular Energies*, Phys. Rev. X **6**, 031007(13) (2016).

[16] A. Kandala et al., *Hardware-efficient variational quantum eigensolver for small molecules and quantum magnets*, Nature **6**, 242 (2017).

[17] F. Neese et al., *Advanced aspects of ab initio theoretical optical spectroscopy of transition metal complexes: Multiplets, spin-orbit coupling and resonance Raman intensities*, Coordination Chemistry Reviews **251**, 288 (2007).

[18] P. Hohenberg and W. Kohn, *Inhomogeneous electron gas*, Phys. Rev. **136 3B**, B864 (1965).

[19] D. Lyakh et al., *Multireference nature of chemistry: The coupled cluster view*, Chem. Rev. **112**, 182 (2012).

[20] S. Bravyi and A. Kitaev, *Fermionic quantum computation*, Annals of Physics **298**, 210 (2002).

[21] J. T. Seeley, M. J. Richard, and P. J. Love, *The Bravyi-Kitaev transformation for quantum computation of electronic structure*, The Journal of Chemical Physics (2012).

[22] J. McClean et al., *OpenFermion: The Electronic Structure Package for Quantum Computers*, arXiv:1710.07629 [quant-ph] (2017).

[23] *Appendix A describes the details of the gate set.*

[24] J. Nelder and R. Mead, *A simplex method for function minimization*, The Computer Journal **7**, 308 (1965).

[25] E. Jones et al., *SciPy: Open source scientific tools for Python*, (2001–).

[26] *The quantumsim package can be found at* `https://github.com/brianzi/quantumsim`.

[27] T. E. O'Brien, B. Tarasinski, and L. DiCarlo, *Density-matrix simulation of small surface codes under current and projective experimental noise*, NPJ Quantum Information , 3 (2017).

[28] A. Blais et al., *Cavity quantum electrodynamics for superconducting electrical circuits: an architecture for quantum computation*, Phys. Rev. A (2004).

[29] J. Koch et al., *Charge-insensitive qubit design derived from the Cooper pair box*, Phys. Rev. A (2007).

[30] J. Preskill, *Fault-tolerant quantum computation*, arXiv: quant-ph/9712048 (1997).

[31] J. R. McClean, M. E. Schwartz, J. Carter, and W. A. de Jong, *Hybrid quantum-classical hierarchy for mitigation of decoherence and determination of excited states*, Phys. Rev. A (2017).

[32] S. Endo, S. C. Benjamin, and Y. Li, *Practical quantum error mitigation for near-future applcations*, arXiv:1712.0971 [quant-ph] (2017).

[33] K. Temme, S. Bravyi, and J. M. Gambetta, *Error mitigation for short-depth quantum circuits*, Phys. Rev. Lett. (2017).

[34] J. I. Colless et al., *Computation of molecular spectra on a quantum processor with an error-resilient algorithm*, Phys. Rev. X , 011021(8) (2017).

[35] Y. Li and S. C. Benjamin, *Efficient variational quantum simulator incorporating active error minimization*, Phys. Rev. X , 021050(14) (2017).